The MOF–driven synthesis of supported palladium clusters with catalytic activity for carbene–mediated chemistry

FRANCISCO R. FORTEA–PÉREZ[1,6], MARTA MON[1,6], JESÚS FERRANDO–SORIA[1], MERCEDES BORONAT[2], ANTONIO LEYVA–PÉREZ[2]*, AVELINO CORMA[2]*, JUAN MANUEL HERRERA[3], DMITRII OSADCHII[4], JORGE GASCON[4], DONATELLA ARMENTANO[5]* AND EMILIO PARDO[1]*

[1]Departamento de Química Inorgánica, Instituto de Ciencia Molecular (ICMOL), Universidad de Valencia, 46980 Paterna, Valencia, Spain

[2]Instituto de Tecnología Química (UPV–CSIC), Universidad Politècnica de València–Consejo Superior de Investigaciones Científicas, Avda. de los Naranjos s/n, 46022 Valencia, Spain

[3]Departamento de Química Inorgánica, Facultad de Ciencias, Universidad de Granada. Avda. Fuentenueva s/n, 18071, Granada, Spain

[4]Catalysis Engineering–Chemical Engineering Dept, Delft University of Technology, Julianalaan 136, 2628 BL Delft

[5]Dipartimento di Chimica e Tecnologie Chimiche, Università della Calabria, 87030 Rende, Cosenza, Italy

[6]These authors contributed equally to this work

e–mail: emilio.pardo@uv.es; donatella.armentano@unical.it; anleyva@itq.upv.es, acorma@itq.upv.es

The development of catalysts able to assist industrially important chemical processes is a topic of high importance. In view of the catalytic capabilities of small metal clusters, research efforts are being focused on the synthesis of novel catalysts bearing such active sites. Here we report a heterogeneous catalyst consisting of Pd_4 clusters with mixed–valence 0/+1 oxidation states, stabilized and homogeneously organized within the walls of a metal-organic framework (MOF). The resulting solid catalyst outperforms state–of–the–art metal catalysts in carbene–mediated reactions of diazoacetates, with high yields (>90%) and turnover numbers (up to 100000). In addition, the MOF–supported Pd_4 clusters retain their catalytic activity in repeated batch and flow reactions (>20 cycles). Our findings demonstrate how this synthetic approach may now instruct the future design of heterogeneous catalysts with advantageous reaction capabilities for other important processes.

Ultrasmall metal clusters[1–5] have attracted a great deal of interest as extremely active and selective catalysts for organic reactions[6,7]. Despite the efforts made, there is yet more work to be done in order to fully understand the exact nature of the catalytic species, their reactivity, structure, shape and nuclearity[8,9]. Ligand stabilization[10] and matrix–supporting[11,12] are the most efficient strategies to synthesize and characterize metal clusters. While the former allows to determine satisfactorily the structure of the cluster metal complex by single crystal X–ray crystallography, these compounds rarely find applications in catalysis[13] since ligand exchange with the reactants triggers decomposition of the cluster. In clear contrast, clusters supported on solids are stable catalytic species with highly reactive uncoordinated atoms[1], but only nuclearity and oxidation state of the metal by X–ray absorption spectroscopies combined with high–resolution microscopies can be addressed. Thus, the synthesis of supported metal clusters with precise topological and electronic properties, as it occurs in metal complexes, would be of much interest.

In this context, Metal–Organic Frameworks (MOFs)[14] have emerged in the last years[15] as very versatile materials for encapsulating catalytic nanosized species within their channels[16]. In addition, the regular and well–defined channels in MOFs appear, theoretically, as the perfect playgrounds to obtain information about the nature of the metallic catalytic species by means of single crystal X–ray crystallography. However, after a number of publications on this topic showing small 1–2 nm metal nanoparticles[17–20], it is difficult to find reports on metal clusters below the nanometre within MOF matrices.

Metal carbenoids are powerful catalytic and synthetic intermediates in organic synthesis, and different metals have been reported to form and transfer carbenes[21]. Despite Pd compounds are found as catalysts for a plethora of fundamental transformations in organic synthesis such as hydrogenations, carbon–carbon couplings, and many others[22], they have been only occasionally employed as catalysts in carbene–transfer processes[23-27].

Here we report the preparation of $Pd^{0/1+}_4$ clusters stabilized by the anionic framework of a MOF. The material is able to catalyse representative carbene–mediated reactions such as the inter– and intra–molecular Buchner ring expansion reaction, the alcohol insertion and the dimerization of diazocompounds, to give some unique naturally–occurring and synthetically–useful products[28-30]. This new catalytic behaviour of Pd lies on the stabilization of the intermediate Pd^+ valence within the supported–MOF cluster, which enables carbene bonding to give a catalytic activity that exceeds in one order of magnitude that of the state–of–the–art catalysts for these reactions. In addition, the solid catalyst can be recovered and reused up to 20 times in batch without any re–activation treatment nor depletion of the catalytic activity, or operated in flow with solvent recycling during hours.

Synthesis and characterization of Pd_4–MOF

Herein, we take advantage of the emerging post–synthetic methods (PSM)[31,32] to synthesize (see Methods), in three steps, $[Pd_4]^{2+}$ clusters from a preformed highly porous anionic MOF

of formula $Mg^{II}_2\{Mg^{II}_4[Cu^{II}_2(Me_3mpba)_2]_3\} \cdot 45H_2O$ (**1**) [Me_3mpba^{4-} = *N,N'*–2,4,6–trimethyl–1,3–phenylenebis(oxamate)] (Fig. 1a) by (*i*) the already reported transmetallation[32] of **1** to yield the more robust MOF $Ni^{II}_2\{Ni^{II}_4[Cu^{II}_2(Me_3mpba)_2]_3\} \cdot 54H_2O$ (**2**) (Fig. 1b), (*ii*) the exchange of the nickel(II) cations hosted in the pores of **1** by $[Pd^{II}(NH_3)_4]^{2+}$ ones yielding the novel compound $[Pd^{II}(NH_3)_4][Pd^{II}_2(\mu\text{–}O)(NH_3)_6)(NH_4)_2]_{0.5}\{Ni^{II}_4[Cu^{II}_2(Me_3mpba)_2]_3\} \cdot 52H_2O$ (**3**) (Fig. 1c) and (*iii*) the reduction process to give the final compound $[Pd_4]_{0.5}@Na_3\{Ni^{II}_4[Cu^{II}_2(Me_3mpba)_2]_3\} \cdot 56H_2O$ (**4**) (Fig. 1d).

Overall, the presence of Pd^{II} cations in a controlled stoichiometry[33,34] together with the confined state provided by the anionic porous network seem to play a key role gaining control of the size and mixed–valence nature of metal particles and thus, such small clusters as $[Pd_4]^{2+}$ units were formed. The robustness of the 3D network, allowed the resolution of the crystal structure of every single material to unambiguously observe the single–crystal to single–crystal guest inclusion and the final observation of quasi–linear $[Pd_4]^{2+}$ clusters (Figs 1, 2 and Supplementary Figs 1–6), reminiscent of ligand–stabilized palladium sandwich complexes reported before[10,35,36], which are undoubtedly stabilized by the network (Figs 1e and 2 and structural details section in the Supplementary Information).

The nature of the Pd_4–MOF compound **4** was established by the combination of a variety of techniques including: density functional theory (DFT) calculations, inductively coupled plasm–mass spectrometry (ICP–MS), elemental, powder X–ray diffraction (PXRD) and thermo–gravimetric (TGA) analyses, Fourier transform infrared (FTIR) under CO and X–ray photoelectron (XPS) spectroscopies and scanning (SEM) and high–resolution transmission electron (HR–TEM) microscopies, including high–angle annular dark field scanning transmission electron microscopy (HAADF–STEM) measurements (Fig. 3, Supplementary Figs 7-17 and Supplementary Table 1). The N_2 adsorption isotherm at 77 K

confirmed the permanent porosity of **4** (Supplementary Fig. 18). Finally, the resolution of the crystal structure of **4** allowed an unambiguous observation of such small Pd entities in **4**.

The anionic $Ni^{II}_4Cu^{II}_6$ open–framework structure displays hydrophilic octagonal pores, exhibiting a virtual diameter of 2.2 nm, that accommodate free nickel(II) cations which can be exchanged afterwards to give **3** and **4** (Figs 1b–d and 2, and Supplementary Figs 1, 2 and 4a) with no evidence of remarkable changes in structural parameters (Supplementary Table 2)[32]. The arrangement of Pd^{2+} moieties in **3** and Pd NCs in **4**, confined into the channels, are strictly related. In **3** they exhibit either mononuclear, $[Pd^{II}(NH_3)_4]^{2+}$, or dinuclear complexes of the type $[Pd^{II}_2(\mu\text{–}O)(NH_3)_6]^{2+}$ (Supplementary Fig. 3), whereas in **4**, after reduction, they finally assemble in centrosymmetric tetranuclear Pd_4 NCs (Fig. 1 and Supplementary Figs 1b, 2 and 4). The Pd^{2+} ions from the ammonia–bridged dinuclear entities in **3** (Supplementary Fig. 3) are tetracoordinated, in a distorted square planar geometry, with Pd–NH_3 and Pd-O bond distances similar to those found in the literature[37]. The Pd atoms in **4** are two– or one–coordinated, respectively in a slightly bent geometry [Pd–Pd–Pd angles of 155(1)° and 169(1)°] (Supplementary Fig. 4) growing tetranuclear NCs. The inner Pd–Pd bond length values [2.57(3)/2.44(3) Å] are significantly shorter than the relatively long outer ones [3.16(2)/2.91(3) Å] though both falling in the range of Pd–Pd bonding interactions[10,35,36,38]. This asymmetry of bond lengths within the $[Pd_4]^{2+}$ moiety is a striking feature, because despite the similarity in the shape of the Pd_4 cluster, such a difference was not observed in the two previously reported ligand–stabilized tetrapalladium compounds, where Pd–Pd separation vary in the range 2.538(1)–2.563(1) Å[35], and 2.571(1)–2.622(1) Å[36].

The possibility to have disordered $[Pd_2]$ instead of $[Pd_4]$ clusters might be consistent and it has been considered. However diverse factors determine that Pd_4 clusters are, by far, the most probable resolution (see structural details section in the Supplementary Information). In order to support the nature of these clusters, theoretical calculations were carried out using

a simplified model of a $Pd_4\{Ni_4[Cu_2(Me_3mpba)_2]_3\}^{2-}$ unit (Fig. 3 and Supplementary Fig. 7). When Pd atoms are allowed to move without restrictions within the octagonal ring model, they approach the donor oxygen atoms of the wall forming bonds with typical Pd–O distances of 2.30/2.37 Å, and optimized Pd–Pd distances of 2.69 and 2.65 Å for the outer and inner bonds, respectively (Fig. 3a). Despite this result apparently contradicts the quasi-linear arrangement of the $[Pd_4]^{2+}$ moiety observed by XRD, averaging of the two equivalent structures obtained from optimization yields a slightly bent, Pd_4 unit with longer outer Pd–Pd distances (Figs. 3b and 3c), in agreement with experiment (Fig. 3d) where the positions of Pd atoms were refined with considerably large thermal motion. Analysis of charge distribution reveals a mixed-valence state of the type $Pd^{+}Pd^{0}Pd^{0}Pd^{+}$, with a calculated net atomic charge of 0.34 and 0.18 e on the outer and inner Pd atoms, respectively.

Fig. 1f suggests a tentative formation mechanism of the Pd_4 NCs by proposing that the $[Pd^{II}_2(\mu\text{–}O)(NH_3)_6]^{2+}$ complexes act as precursors of the central NCs core, whereas the mononuclear Pd^{2+} cations become the terminal atoms in the Pd_4 NCs (Supplementary Fig. 3e). Finally, hydrated charge–counterbalancing alkali Na^{+} cations are present in **4** as a result of the reduction with $NaBH_4$. They are distributed within the channels, further stabilizing the whole net (Supplementary Fig. 5).

The Pd^{2+}–based guest molecules in **3**, are efficiently organized within the MOF pore, where they can react, aggregating in ordered dimers. This suggests that the crystalline porous host *aligns* the molecules within its cavities through a high degree of molecular recognition. While in **3**, $[Pd^{II}_2(\mu\text{–}O)(NH_3)_6]^{2+}$ dimers interact with the net through $\text{–}NH_3\cdots O$ hydrogen bonds (Supplementary Fig. 6), in **4**, tetranuclear $[Pd_4]^{2+}$ clusters are most-likely stabilized either by the network, through weak supramolecular interactions between Pd and oxamate moieties, or through a probable hydrated primary coordination sphere around Pd atoms, hydrogen-bonded to the net (Figs 1f and 2 and Supplementary Fig. 4). Despite the typical

structural uncertainty related to the difficulty to determine the positions of solvent molecules in porous materials, the most plausible $[Pd_4]^{2+}$ cluster structure is solvated and stabilized by a synergic effect between the network and the solvent molecules surrounding clusters. The large accessible free voids (56% of the total cell volume) allow the guest to become more than an innocent bystander. Such a vastly solvated nano-confined space, stabilizes catalytic NCs without protective groups while retaining access to reactant species.

Powder X–ray diffraction (PXRD) patterns of **3** and **4** (Supplementary Fig. 8) confirm the crystallinity and pureness of the bulk samples with no trace of the typical peaks of Pd NPs, not even after catalysis.

FTIR spectroscopy of adsorbed CO[39] is able to differentiate between supported Pd^0, Pd^+ and Pd^{2+}. The spectrum of **4** (Supplementary Fig. 10a) shows absorption bands at 2140 cm^{-1} and 1882 cm^{-1}, which correspond to linearly adsorbed CO to Pd^+ and Pd^0, respectively, together with some weak bands assignable to Pd^{2+} metal cations.[39-41] For the sake of comparison, the FTIR spectrum of adsorbed CO on the mono–directional zeolite LH after impregnation and reduction of Pd^{2+} was recorded (Supplementary Fig. 10b), showing that the mono–directional zeolite is able to stabilize Pd^+ in much lesser extent.

The XPS spectrum of compound **3** is shown in Supplementary Fig. 11a. The Pd3d line consists of only one doublet with binding energy (BE) of $Pd3d_{5/2}$ peak equal to 338.6 eV, corresponding to Pd(II).[42] In turn, the XPS of **4** (Supplementary Fig. 11b), after deconvolution of the Pd3d line, shows the typical peak for Pd^0 at a binding energy of $BE(Pd3d_{5/2})$ = 335.7 eV together with a non–ordinary signal at $BE(Pd3d_{5/2})$ = 337.0 eV, an energy between that of Pd^0 and the residual signals of Pd^{2+} at $BE(Pd3d_{5/2})$ = 338.7 eV, and with a 1:1 ratio respect to Pd^0, which, even if distinguishing between Pd^0 and Pd^+ is challenging, can be attributed to Pd^+, as previously reported[42].

All these results, together, further support that both Pd^{+} and Pd^{0} can be found in **4** and that the $Pd^{+}Pd^{0}Pd^{0}Pd^{+}$ arrangement predicted by theoretical calculations, is the most probable electronic state of the cluster.

Aberration corrected HR–TEM images of **4** (Supplementary Figs 12a, 13 and 14) reveal no aggregation of the Pd_4 NCs and their uniform distribution throughout the highly crystalline framework. Analysis of these images also directly visualizes the lattice fringes of the net, where the interplanar spacing is 0.248 nm (Supplementary Fig. 12a) corresponding to (110) planes of the MOF and confirm its retained crystallinity. Both, SEM and HAADF–STEM imaging and their corresponding EDX elemental mappings for Cu, Ni, Pd and Na elements (Supplementary Figs 12b,d and 15–17) confirm a homogeneous spatial distribution of the Pd_4 NCs through the MOF crystal.

Pd_4–MOF catalyses carbene–transfer reactions.

Table 1 shows the catalytic results of different Pd compounds for the Buchner reaction of benzene derivatives to give naturally–occurring and synthetically–useful cycloheptatrienes.[28] This unique transformation is catalysed only by dirhodium salts[29] or particular copper complexes.[30] Here, from the different Pd compounds tested that include salts, complexes, pure metallic forms, and different Pd supported species (entries 1–26), only **3** and **4** (entries 27–28) catalyse efficiently the intermolecular Buchner reaction of benzene **5a** and ethyl diazoacetate **6a** (Table 1 left) and the intramolecular reaction of **8** (Table 1 right).

Kinetic analysis showed that the green solid **3** gives an induction time of ~30 min after which the intermolecular reaction starts and proceeds (Supplementary Fig. 19), and *in–situ* magic angle spinning–solid nuclear magnetic resonance (MAS–NMR) of a sample of **3** treated with an equimolecular amount respect to Pd of isotopically–labelled **6a** $N_2{}^{13}CH–COOEt$[43-44], in gas phase, shows the immediate transformation of **6a** to the corresponding dimer (Supplementary Fig. 20) with the recovered solid active for the Buchner reaction

without induction period. These results point to diazoacetate **6a** as a reducing agent of Pd^{2+} in **3**, to give **4** under reaction conditions, as $NaBH_4$ does externally. The solid precursors **1** and **2** do not show any catalytic activity, which confirm that the catalytic activity comes from $[Pd_4]^{2+}$ and not from any defects on the MOF structure.

Zeolites capable to stabilize Pd^+ cluster species within their anionic zeolite framework, such as KL and mordenite, give significant yields of **7a** (entries 23–26), which supports the active role of Pd^+ in the reaction. In contrast, ligand-stabilised complexes such as a perylene–stabilized linear $[Pd_4]^{2+}$ complex (**10d**)[35,45] and two commercially–available phosphine–stabilized Pd^+ dimer complexes, **10e**[46] and **10f**[47] were prepared and evaluated catalytically (entries 29-31). In all cases, product **7a** was not observed, which can be easily understood taking into account that the labile perylene ligand (**10d**) is also a potential reactant in the Buchner reaction and that **10d–f** are temperature–sensitive compounds.

The catalytic amount of **4** could be lowered to 0.5 mol% and reused up to 20 times without a significant depletion of its inherent catalytic activity for the intermolecular reaction (entry 32, Supplementary Fig. 21). The process could also be run in flow (Supplementary Fig. 22) by adding **6a** with a syringe pump to a fixed amount of catalyst **4** under recirculating benzene **5a**. In this way, a solution of ~1 gram of **7a** in 100 ml of benzene (~0.1 M) could be obtained, which not only saves 5–fold amounts of benzene but also enables a safer handling of **6a** for industrial applications[30,48]. Besides, the recovered catalyst **4** completely retained its intrinsic catalytic activity after working in flow mode for 24 hours (Supplementary Fig. 23). A TON >2000 was obtained for **4** either in batch or in flow, a value one order of magnitude higher than the state–of–the–art–catalyst $Rh_2(OAc)_4$ (TON= 104, entry 33) which rapidly decomposes to inactive species after the first use[29].

Fig. 4 shows that **4** catalyses the intermolecular Buchner reaction of different arenes and diazoacetates in yields comparable to $Rh_2(OAc)_4$[29]. In contrast to the soluble catalyst, the

isomeric distribution obtained with **4** for products **7a–l** shifts significantly towards less hindered products (Supplementary Table 3). For instance, the isomeric ratio at full conversion for the 2–, 3– and 4–methyl substituted products in **7b** changes from ~1:1:2.5 with $Rh_2(OAc)_4$ or ~1:1:6 with $Rh_2(OAc_{3-F})_4$[29] to 0:1:1 with **4**, indicating that the MOF structure imposes shape selectivity effects during the catalytic process. Indeed, the intramolecular Buchner reaction of the bulkier diazoacetate **8**[49] proceeds in 57% yield, a significant lower value than the intermolecular reaction, since the channel of **4** probably restricts sterically the transition state. Notice that no conversion of **8** was found with KL and mordenite with smaller ~7 $Å^2$ channels.

The reaction rate for the intermolecular Buchner reaction of **5a** (Supplementary Fig. 24) follows a first order kinetics with respect to both reactants and catalyst to give the equation rate $v_0=k$[cat][**5a**][**6a**] (k=observable kinetic constant) at low concentrations of **6a**. The participation of a Pd carbenoid in the rate–determining step of the reaction is supported by: 1) the similar rates found for N_2 liberation and formation of cycloheptatriene **7a**, 2) values for $\Delta H^{\neq}$ and $\Delta S^{\neq}$ of 19.0(8) kcal mol^{-1} and -9.9(5) kcal mol^{-1} K^{-1}, respectively, obtained by an Eyring plot of the intermolecular reaction and which agree with previous reports on associative transition states during this reaction[50], and 3) the structure of the conjugated cycloheptatrienes obtained here can only come, in principle, from the classically accepted cyclopropanation/electrocyclic ring opening route, since other potential ways of coupling/opening should lead to different products. Thus, a plausible mechanism for the Pd_4–catalysed Buchner reaction can be proposed (Fig. 5). The reaction would start with the formation of a Pd carbenoid, which enables the cyclopropanation of the arene and the 6π disrotatory electrocyclic ring opening of the so–formed norcaradiene, to give the final cycloheptatriene product.

Finally, Fig. 4 also compares the catalytic activity of different Pd compounds for other representative carbene–transfer mediated reactions of diazocompounds, such as the insertion of alcohols or the dimerization. The results show that 0.005 mol% of **4** gives >90% yield of products **12a–f** and **13a–d** with TONs approaching 100 000 catalytic cycles in some cases, thus outperforming not only other Pd catalysts but also the state–of–the–art metal catalysts for these reactions[29,30].

CONCLUSIONS

The confinement and protection provided by the MOF together with an exquisite control of the stoichiometry of the Pd^{2+} cations has allowed the multi–gram scale synthesis of linear $Pd^{0/1+}{}_4$ clusters, homogenously distributed and stabilized along the MOF channels and fully characterised with X–ray crystallography. These ultrasmall clusters catalyse very efficiently representative carbene–mediated reactions such as the inter– and intramolecular Buchner reaction, the O–H insertion and the dimerization of diazocompounds, with TONs at least one order of magnitude higher that the state of the art most active catalysts. The solid $Pd^{0/1+}{}_4$–MOF catalyst is very stable under reaction conditions, recoverable and reusable, and can work in a batch or in flow with no observable loss of activity with time. These results bring Pd to the selected group of metals that catalyse carbene–mediated reactions.

REFERENCES

1. Argo, A. M., Odzak, J. F., Lai, F. S. & Gates, B. C. Observation of ligand effects during alkene hydrogenation catalysed by supported metal clusters. *Nature* **415,** 623–626 (2002).
2. Corma, A. *et al.* Exceptional oxidation activity with size-controlled supported gold clusters of low atomicity. *Nat. Chem.* **5,** 775–781 (2013).
3. Oliver-Meseguer, J., Cabrero-Antonino, J. R., Dominguez, I., Leyva-Perez, A. & Corma, A. Small Gold Clusters Formed in Solution Give Reaction Turnover Numbers of 107 at Room Temperature. *Science.* **338,** 1452–1455 (2012).
4. Wang, N. *et al.* In Situ Confinement of Ultrasmall Pd Clusters within Nanosized Silicalite-1 Zeolite for Highly Efficient Catalysis of Hydrogen Generation. *J. Am. Chem. Soc.* **138,** 7484–7487 (2016).

5. Yamamoto, K. *et al.* Size-specific catalytic activity of platinum clusters enhances oxygen reduction reactions. *Nat. Chem.* **1,** 397–402 (2009).

6. Boronat, M., Leyva-Pérez, A. & Corma, A. Theoretical and Experimental Insights into the Origin of the Catalytic Activity of Subnanometric Gold Clusters: Attempts to Predict Reactivity with Clusters and Nanoparticles of Gold. *Acc. Chem. Res.* **47,** 834–844 (2014).

7. Campbell, C. T. The Effect of Size-Dependent Nanoparticle Energetics on Catalyst Sintering. *Science.* **298,** 811–814 (2002).

8. Lei, Y. *et al.* Increased Silver Activity for Direct Propylene Epoxidation via Subnanometer Size Effects. *Science.* **328,** 224–228 (2010).

9. Tyo, E. C. & Vajda, S. Catalysis by clusters with precise numbers of atoms. *Nat. Nanotechnol.* **10,** 577–588 (2015).

10. Murahashi, T. Discrete Sandwich Compounds of Monolayer Palladium Sheets. *Science.* **313,** 1104–1107 (2006).

11. Liu, L. *et al.* Generation of subnanometric platinum with high stability during transformation of a 2D zeolite into 3D. *Nat. Mater.* **16**, 132–138 (2017).

12. Serna, P. & Gates, B. C. Molecular Metal Catalysts on Supports: Organometallic Chemistry Meets Surface Science. *Acc. Chem. Res.* **47,** 2612–2620 (2014).

13. Okrut, A. *et al.* Selective molecular recognition by nanoscale environments in a supported iridium cluster catalyst. *Nat. Nanotechnol.* **9,** 459–465 (2014).

14. Furukawa, H., Cordova, K. E., O'Keeffe, M. & Yaghi, O. M. The Chemistry and Applications of Metal-Organic Frameworks. *Science.* **341,** 974 (2013).

15. Gascon, J., Corma, A., Kapteijn, F. & Llabrés i Xamena, F. X. Metal Organic Framework Catalysis: Quo vadis ? *ACS Catal.* **4,** 361–378 (2014).

16. Moon, H. R., Lim, D.-W. & Suh, M. P. Fabrication of metal nanoparticles in metal–organic frameworks. *Chem. Soc. Rev.* **42,** 1807–1824 (2013).

17. Li, X. *et al.* Controlling Catalytic Properties of Pd Nanoclusters through Their Chemical Environment at the Atomic Level Using Isoreticular Metal–Organic Frameworks. *ACS Catal.* **6,** 3461–3468 (2016).

18. Liu, H. *et al.* Controllable Encapsulation of 'Clean' Metal Clusters within MOFs through Kinetic Modulation: Towards Advanced Heterogeneous Nanocatalysts. *Angew. Chem., Int. Ed.* **55,** 5019–5023 (2016).

19. Liu, L. *et al.* Size-confined growth of atom-precise nanoclusters in metal–organic frameworks and their catalytic applications. *Nanoscale* **8,** 1407–1412 (2016).

20. Yang, Q., Xu, Q., Yu, S.-H. & Jiang, H.-L. Pd Nanocubes@ZIF-8: Integration of Plasmon-Driven Photothermal Conversion with a Metal-Organic Framework for Efficient and Selective Catalysis. *Angew. Chem., Int. Ed.* **55,** 3685–3689 (2016).

21. Seidel, G. & Fürstner, A. Structure of a Reactive Gold Carbenoid. *Angew. Chem., Int. Ed.* **53,** 4807–4811 (2014).

22. Wu, X.-F., Anbarasan, P., Neumann, H. & Beller, M. From Noble Metal to Nobel Prize: Palladium-Catalyzed Coupling Reactions as Key Methods in Organic Synthesis. *Angew. Chem., Int. Ed.* **49,** 9047–9050 (2010).

23. Albéniz, A. C., Espinet, P., Manrique, R. & Pérez-Mateo, A. Observation of the Direct Products of Migratory Insertion in Aryl Palladium Carbene Complexes and Their

Subsequent Hydrolysis. *Angew. Chem., Int. Ed.* **41,** 2363–2366 (2002).

24. Fillion, E. & Taylor, N. J. Cine -Substitution in the Stille Coupling: Evidence for the Carbenoid Reactivity of sp 3 - g em -Organodimetallic Iodopalladio-trialkylstannylalkane Intermediates. *J. Am. Chem. Soc.* **125,** 12700–12701 (2003).
25. Qin, G., Li, L., Li, J. & Huang, H. Palladium-Catalyzed Formal Insertion of Carbenoids into Aminals via C–N Bond Activation. *J. Am. Chem. Soc.* **137,** 12490–12493 (2015).
26. Solé, D., Mariani, F., Bennasar, M.-L. & Fernández, I. Palladium-Catalyzed Intramolecular Carbene Insertion into C(sp 3)−H Bonds. *Angew. Chem., Int. Ed.* **55,** 6467–6470 (2016).
27. Gutiérrez-Bonet, Á., Juliá-Hernández, F., de Luis, B. & Martin, R. Pd-Catalyzed C(sp 3)–H Functionalization/Carbenoid Insertion: All-Carbon Quaternary Centers via Multiple C–C Bond Formation. *J. Am. Chem. Soc.* **138,** 6384–6387 (2016).
28. McKervey, M. A., Tuladhar, S. M. & Twohig, M. F. Efficient synthesis of bicyclo[5.3.0]decatrienones and of 2-tetralones via rhodium(II) acetate-catalysed cyclisation of α-diazoketones derived from 3-arylpropionic acids. *J. Chem. Soc., Chem. Commun.* 129–130 (1984).
29. Anciaux, A. J. *et al.* Transition-metal-catalyzed reactions of diazo compounds. 2. Addition to aromatic molecules: catalysis of Buchner's synthesis of cycloheptatrienes. *J. Org. Chem.* **46,** 873–876 (1981).
30. Maestre, L. *et al.* A fully recyclable heterogenized Cu catalyst for the general carbene transfer reaction in batch and flow. *Chem. Sci.* **6,** 1510–1515 (2015).
31. Brozek, C. K. & Dincă, M. Cation exchange at the secondary building units of metal-organic frameworks. *Chem. Soc. Rev.* **43,** 5456–67 (2014).
32. Grancha, T. *et al.* Postsynthetic Improvement of the Physical Properties in a Metal-Organic Framework through a Single Crystal to Single Crystal Transmetallation. *Angew. Chem., Int. Ed.* **54,** 6521–6525 (2015).
33. Mon, M. *et al.* Selective Gold Recovery and Catalysis in a Highly Flexible Methionine-Decorated Metal–Organic Framework. *J. Am. Chem. Soc.* **138,** 7864–7867 (2016).
34. Mon, M. *et al.* Selective and Efficient Removal of Mercury from Aqueous Media with the Highly Flexible Arms of a BioMOF. *Angew. Chem., Int. Ed.* **55,** 11167–11172 (2016).
35. Murahashi, T., Uemura, T. & Kurosawa, H. Perylene−Tetrapalladium Sandwich Complexes. *J. Am. Chem. Soc.* **125,** 8436–8437 (2003).
36. Murahashi, T., Kato, N., Uemura, T. & Kurosawa, H. Rearrangement of a Pd4 Skeleton from a 1D Chain to a 2D Sheet on the Face of a Perylene or Fluoranthene Ligand Caused by Exchange of the Binder Molecule. *Angew. Chem., Int. Ed.* **46,** 3509–3512 (2007).
37. Mealli, C. *et al.* Theoretical Aspects of the Heterobimetallic Dimers with the T Over Square Structural Motif. Synthesis and Structure of a Heteronuclear Platinum and Palladium Complex with 1-Methylcytosinato Bridging Ligands. *Inorg. Chem.* **34,** 3418–3424 (1995).
38. Murahashi, T. & Kurosawa, H. Organopalladium complexes containing palladium-palladium bonds. *Coord. Chem. Rev.* **231,** 207–228 (2002).

39. Fernández-García, M. *et al.* Role of the state of the metal component on the light-off performance of Pd-based three-way catalysts. *J. Catal.* **221,** 594–600 (2004).

40. Liang, B., Zhou, M. & Andrews, L. Reactions of laser-ablated Ni, Pd, and Pt Atoms with carbon monoxide: Matrix infrared spectra and density functional calculations on $M(CO)_n$ (n= 1-4), $M(CO)_n$ (n= 1-3), and $M(CO)_n^+$ (n= 1-2), (M= Ni, Pd, Pt). *J. Phys. Chem. A* **104**, 3905–3914 (2000).

41. Willner, H., Bodenbinder,M., Bröchler, R., Hwang, G., Rettig, S. J., Trotter, J., Ahsen, B., Westphal, U., Jonas, V., Thiel, W., Aubke, F. Superelectrophilic tetrakis(carbonyl)palladium(II)- and -platinum(II) undecafluorodiantimonate(V), $[Pd(CO)_4][Sb_2F_{11}]_2$ and $[Pt(CO)_4][Sb_2F_{11}]_2$: syntheses, physical and spectroscopic properties, their crystal, molecular, and extended structures, and density functional calculations: an experimental, computational, and comparative study. *J. Am. Chem. Soc.* **123***,* 588–602 (2001).

42. Nefedov, V. I. *et al.* ESCA and X-ray spectral study of Pd(0), Pd(I) and Pd(II) compounds with triphenylphosphine ligands. *Inorganica Chim. Acta* **35,** L343–L344 (1979).

43. Searle, N. E. Ethyl Diazoacetate. *Org. Synth.* **36,** 25 (1956).

44. Ranocchiari, M. & Mezzetti, A. Ru/PNNP-Catalyzed Asymmetric Imine Aziridination by Diazo Ester Activation. *Organometallics* **28,** 3611–3613 (2009).

45. Horiuchi, S. *et al.* Multinuclear metal-binding ability of a carotene. *Nat. Commun.* **6,** 6742 (2015).

46. Barder, T. E. Synthesis, Structural, and Electron Topographical Analyses of a Dialkylbiaryl Phosphine/Arene-Ligated Palladium(I) Dimer: Enhanced Reactivity in Suzuki−Miyaura Coupling Reactions. *J. Am. Chem. Soc.* **128,** 898–904 (2006).

47. Yin, G., Kalvet, I. & Schoenebeck, F. Trifluoromethylthiolation of Aryl Iodides and Bromides Enabled by a Bench-Stable and Easy-To-Recover Dinuclear Palladium(I) Catalyst. *Angew. Chem., Int. Ed.* **54,** 6809–6813 (2015).

48. Maas, G. New Syntheses of Diazo Compounds. *Angew. Chem., Int. Ed.* **48,** 8186–8195 (2009).

49. Kennedy, M., McKervey, M. A., Maguire, A. R., Tuladhar, S. M. & Twohig, M. F. The intramolecular Buchner reaction of aryl diazoketones. Substituent effects and scope in synthesis. *J. Chem. Soc. Perkin Trans. 1* 1047 (1990).

50. Pereira, A. *et al.* Copper-Carbene Intermediates in the Copper-Catalyzed Functionalization of O-H Bonds. *Chem. - A Eur. J.* **21,** 9769–9775 (2015).

METHODS

Methods and any associated references are available in the online version of the paper.

PREPARATION

Materials. All chemicals were of reagent grade quality. They were purchased from commercial sources and used as received. Crystals of $Mg_2^{II}\{Mg^{II}_4[Cu^{II}_2(Me_3mpba)_2]_3\} \cdot 45H_2O$ (**1**), $Ni_2^{II}\{Ni^{II}_4[Cu^{II}_2(Me_3mpba)_2]_3\} \cdot 54H_2O$ (**2**) and $[Pd(NH_3)_4]Cl_2$ were prepared as previously reported (see Supplementary Methods). Alternatively, a large scale synthesis of $Ni_2^{II}\{Ni^{II}_4[Cu^{II}_2(Me_3mpba)_2]_3\} \cdot 54H_2O$ (**2**) was carried out by direct reaction of two aqueous solutions (250 mL each) of $Na_4[Cu_2(Me_3mpba)_2] \cdot 4H_2O$ (8.71 g, 0.010 mol) and $Ni(NO_3)_2 \cdot 6H_2O$ (3.88 g, 0.013 mol) and subsequent addition, after filtration and re–suspension in 150 mL water of the resulting compound, of 1.94 g (0.0067 mol) of $Ni(NO_3)_2 \cdot 6H_2O$ (Yield 99 %).

$[Pd^{II}(NH_3)_4][Pd^{II}_2(\mu\text{–}O)(NH_3)_6(NH_4)_2]_{0.5}\{Ni^{II}_4[Cu^{II}_2(Me_3mpba)_2]_3\} \cdot 52H_2O$ (3): Well–formed deep green prisms of **3**, which were suitable for X–ray diffraction, were obtained by immersing crystals of **2** (*ca*. 5 mg, 0.0015 mmol) for 48 hours in 5 mL of a $[Pd(NH_3)_4]Cl_2$ aqueous solution (0.004 mmol). Aiming at industrial applications, a multigram scale procedure was also carried out by using the same synthetic procedure but with greater amounts of both, a powder sample of compound **2** (20 g, 5.8 mmol) and $[Pd(NH_3)_4]Cl_2$ (3.43 g, 14.0 mmol), with the same successful results and a very high yield (20.33 g, 96%). Anal.: calcd (%) for $Cu_6Ni_4Pd_2C_{78}H_{189}N_{20}O_{88.5}$ (3652.3): C, 25.65; H, 5.22; N, 7.67. Found: C, 25.68; H, 5.13; N, 7.33. IR (KBr): ν = 3014, 2951 and 2913 cm^{-1} (C–H), 1607 cm^{-1} (C=O).

$[Pd_4]_{0.5}@Na_3\{Ni^{II}_4[Cu^{II}_2(Me_3mpba)_2]_3\} \cdot 56H_2O$ (4): Both, crystals (*ca*. 5 mg) and a powder polycrystalline sample of **3** (*ca*. 10 g), were suspended in 50 mL of a H_2O/CH_3OH (1:2) solution to which an excess of $NaBH_4$, divided 26 in fractions (each fraction consisting of 1 mole of $NaBH_4$ per mole of **3** to give a final $NaBH_4$ / MOF molar ratio of 26 or, which is the same, $NaBH_4$ / Pd atom molar ratio of 13), was added progressively in the space of 72 hours. After each addition, the mixture was allowed to react for 1.5 hour. After this period, samples were gently washed with a H_2O/CH_3OH solution and filtered on paper giving excellent yields (98%). Anal.: calcd (%) for $Cu_6Ni_4Pd_2Na_3C_{78}H_{172}N_{12}O_{92}$ (3648.1): C, 25.68; H, 4.75; N, 4.61.

Found: C, 25.68; H, 4.63; N, 4.65. IR (KBr): ν = 3013, 2964 and 2914 cm^{-1} (C–H), 1603 cm^{-1} (C=O).

SINGLE CRYSTAL X–RAY DIFFRACTION

Crystal data for **3** and **4**: tetragonal, space group *P*4/*mmm*, $T = 90(2)$ K, $Z = 4$; **3**: $C_{78}H_{189}Cu_6N_{20}Ni_4O_{88.5}Pd_2$, $a = 35.920(2)$ Å, $c = 15.3561(9)$ Å, $V = 19813(2)$ $Å^3$, $\rho_{calc} = 1.224$ $g.cm^{-3}$, $\mu = 1.259$ mm^{-1}; **4**: $C_{78}H_{172}Cu_6N_{12}Na_3Ni_4O_{92}Pd_2$, $a = 35.794(13)$ Å, $c = 15.063(5)$ Å, $V = 19298(16)$ $Å^3$, $\rho_{calc} = 1.256$ $g.cm^{-3}$, $\mu = 1.299$ mm^{-1}. Further details can be found at the Supplementary Information.

X–RAY POWDER DIFFRACTION MEASUREMENTS

PXRD patterns of solid polycrystalline samples **3** and **4**, before and after catalysis, were obtained with a Empyrean PANalytical powder diffractometer, using Cu Kα radiation (λ = 1.54056 Å) at room temperature (2θ = 2–60°).

FTIR SPECTROSCOPY OF ADSORBED CO

The spectra were recorded on a Biorad FTS–40A spectrometer equipped with a DTGS detector. The experiments have been carried out in a homemade IR cell able to work in the high and low (77 K) temperature range. Further experimental details can be found in the Supplementary Methods.

MICROSCOPY MEASUREMENTS

High–Resolution Transmission Electron Microscopy (HR–TEM), High–Angle Annular Dark–Field Scanning Transmission Electron microscopy (HAADF–STEM) and Energy Dispersive X–Ray Analysis (EDX) characterizations were done using a HAADF–FEI–

TITAN G2 electron microscope. 5 mg of the material was re–dispersed in 1 mL of absolute EtOH. Carbon reinforced copper grids (200 meshs) were submerged into the suspension 30 times and then allowed to dry on air for 24 h.

Scanning Electron Microscopy coupled with Energy Dispersive X–ray (SEM/EDX) was carried out with a XL 30 ESEM (PHILIPS) microscope equipped with a home–made EDX energy dispersive X–ray detector.

X–RAY PHOTOELECTRON SPECTROSCOPY MEASUREMENTS

Samples were prepared by dropping a solid water suspension onto a molybdenum plate followed by air drying, and then measurements were performed on a SPECS spectrometer equipped with a Phoibos 150 MCD–9 analyser using non–monochromatic Mg KR (1253.6 eV) X–ray source working at 50 W. As an internal reference for the peak positions in the XPS spectra, the C1s peak has been set at 284.5 eV.

MAGIC ANGLE SPINNING–SOLID NUCLEAR MAGNETIC RESONANCE

50 mg of catalyst **3** were introduced into glass inserts and dehydrated at 80 °C during 18 h. Then, 4.7 μmol of isotopically–labelled **6a** $N_2{}^{13}CH$–COOEt, corresponding to Pd/**6a**=1, were introduced onto the dehydrated material. The glass inserts were sealed while they were immersed into liquid nitrogen. In-situ ^{13}C Solid–state NMR spectra were recorded at room temperature with a Bruker AVIII HD 400 WB spectrometer. The glass inserts were fitted into 7 mm rotors and were spun at 5 kHz in a Bruker BL7 probe. ^{13}C CP/MAS NMR spectra were recorded with proton decoupling, with ^{1}H 90° pulse length of 5 μs, and a recycle delay of 3s.

COMPUTATIONAL DETAILS

All calculations are based on Density Functional Theory (DFT) and were carried out with the Gaussian 09 program package, using the hybrid B3PW91 functional, the LANL2DZ basis set

for Pd, Cu and Ni atoms, and the standard 6-311G(d,p) basis set by Pople for O, N, C and H atoms. Atomic charges were calculated using the natural bond order (NBO) approach. A detailed description of models and methods is given in the Supplementary Information.

CATALYTIC EXPERIMENTS

A detailed description of all the catalytic experiments is given in the Supplementary Information.

DATA AVAILABILITY

All data supporting the findings of this work are available from the corresponding authors on request.

Crystallographic data for the structure reported in this paper have been deposited in the Cambridge Structural Database with CCDC numbers 1517224–1517225.

Acknowledgements

This work was supported by the MINECO (Spain) (Projects CTQ2013–46362–P, CTQ2014–56312–P and Excellence Units "Severo Ochoa" and "Maria de Maeztu" SEV–2012–0267 and MDM–2015–0538), the Generalitat Valenciana (Spain) (Project PROMETEOII/2014/070), the Ministero dell'Istruzione, dell'Università e della Ricerca (Italy) and the Junta de Andalucía (FQM–195 and P11–FQM–7756). M. M. thanks the MINECO for a predoctoral contract. Thanks are also extended to the Ramón y Cajal Program and the "Convocatoria 2015 de Ayudas Fundación BBVA a Investigadores y Creadores Culturales" (E. P., A. L.–P. and J. F.–S.). J.G. acknowledge the financial support of the European Research Council under

the European Union´s Seventh Framework Programme (FP/2007–2013) / ERC Grant Agreement n. 335746, CrystEng–MOF–MMM.

Author contributions

Author contributions are as follows: E. P., A. L.–P., A. C. and D. A., designed the research; E. P. and J. F., coordinated the whole work; F. F.–P. and M. M., performed synthetic work; D. A. performed powder and single–crystal XRD characterisation and analysed data; A. L.–P. carried out the catalytic experiments; J. G. and D. O. performed spectroscopic characterisation and analysed data; J. M. H. performed microscopy measurements; M. B. carried out the theoretical calculations; E. P., A. L.–P., A. C., D. A. J. F.–S, M. B. and J. G. wrote and revised the paper.

Competing financial interests

The authors declare that they have no competing financial interests.

FIGURE LEGENDS

FIGURE 1 X–ray crystal structure. a–**d**. Design approach showing the structures of **1**–**4** determined by single–crystal X–ray diffraction from the three–step PS process consisting of a transmetallation **1** (**a**) to give **2** (**b**), an exchange of the Ni^{II} cations of the pores by $[Pd^{II}(NH_3)_4]^{2+}$ ones yielding **3** (**c**) and the final reduction process affording **4** (**d**). **e**. Perspective views of a channel of **4** along the *c* (left) and *a* (right) axis. **f**. Detail of the proposed self-assembly after reduction process of the Pd^{II} units in **3** (left) to give the Pd_4 cluster in **4** (right). Copper, magnesium and nickel atoms from the network are represented by cyan, orange and yellow polyhedral, respectively, whereas organic ligands are depicted as sticks. Orange, yellow, pink, dark blue, pale blue and red spheres represent Mg, Ni, Na and Pd atoms and NH_3 and O^{2-} molecules/ions, respectively. Dashed and dotted lines represent the Pd···O and Na···O weak supramolecular interactions, respectively.

FIGURE 2 Clusters X-ray structure. Perspective view along *b* crystallographic axis of two portions (**a** and **b**) of crystal structure of **4** enclosing the two crystallographic not equivalent ligand–stabilized quasi–linear $[Pd_4]^{2+}$ NCs. MOF structure is depicted as gold sticks and Pd atoms are represented as purple spheres. Purple dotted lines show some of the cluster–network interactions.

FIGURE 3 Density functional theory calculations. Optimized geometry of Pd_4 in a $Pd_4\{Ni_4[Cu_2(Me_3mpba)_2]_3\}^{2-}$ model. The two equivalent structures separated (**a**) overlapped (**b**) and averaged (**c**) are shown, together with the XRD structure (**d**). Pd-Pd and Pd-O (*italics*) distances are given in Å. Pd, Cu, Ni, N, O, C and H atoms are depicted in blue, green, pink, purple, red, orange and white, respectively.

Table 1. **Catalytic results for Buchner reactions and structures of the Pd complexes tested 10a–f.**

Reaction conditions: **6** (15 μl, 0.14 mmol, inter–) or **8** (100 mg, 0.60 mmol, intra–) in the corresponding solvent (6 ml) at reflux temperature with the Pd catalyst (5 and 1 mol%, respectively) for 2 h. Under the indicated reaction conditions, conversion of the diazoacetate is always 100%, either to the desired products, alkene dimers, protonation to the acetate, and/or unidentified decomposition products. Reaction yields were triple–checked by *in–situ* ^{1}H–NMR analysis in deuterated solvents after calibration with the pure products, GC–MS analysis after derivatization to the more stable conjugated isomers with CF_3COOH or Et_3N and calibration with the pure products,[57] and isolated yields. Given yields refers to the average with a ±5% error. [a] 6 h reaction time; between brackets pump addition of the diazocompound.

FIGURE 4 Scope and catalytic results.

Top Scope for the Pd_4 catalysed intermolecular Buchner reaction. **Bottom**. Catalyst comparison and substrate scope for other Pd_4–catalysed carbene–mediated reactions of diazoacetates. Under the indicated reaction conditions, conversion of the diazoacetate is always 100%, either to the desired products, protonation to the acetate, and/or unidentified decomposition products.

FIGURE 5 Proposed mechanism for Pd_4 catalysed intermolecular Buchner reaction.

FIGURE 1 X–ray crystal structure

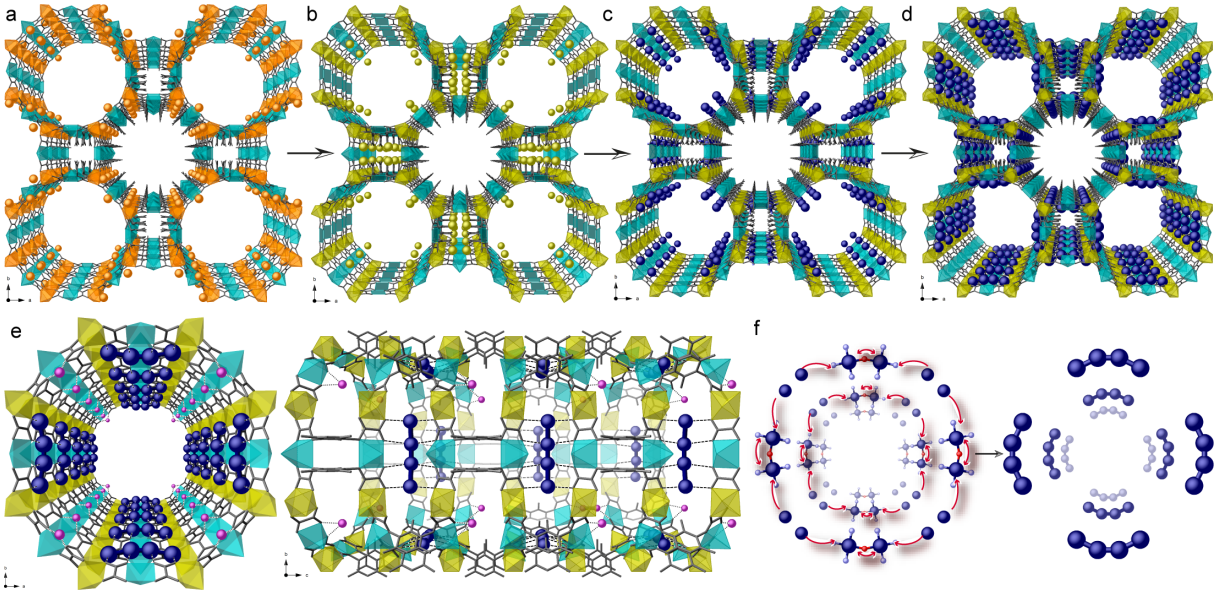

FIGURE 2 Clusters X-ray structure

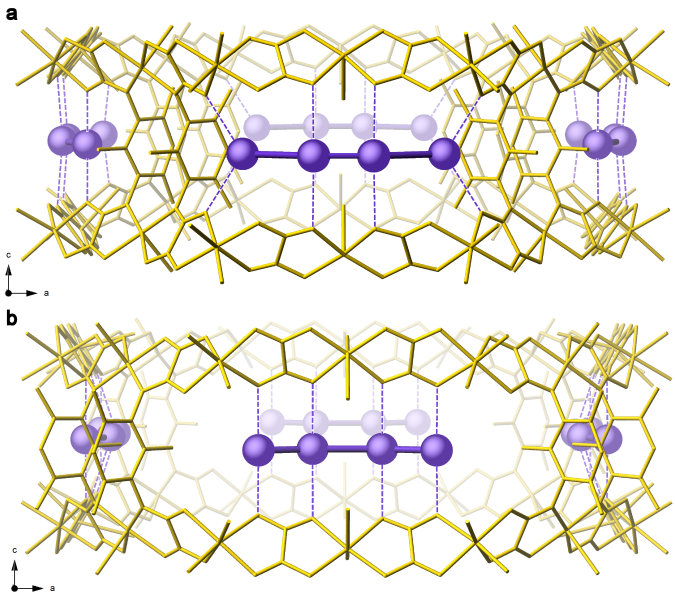

FIGURE 3 Density functional theory calculations.

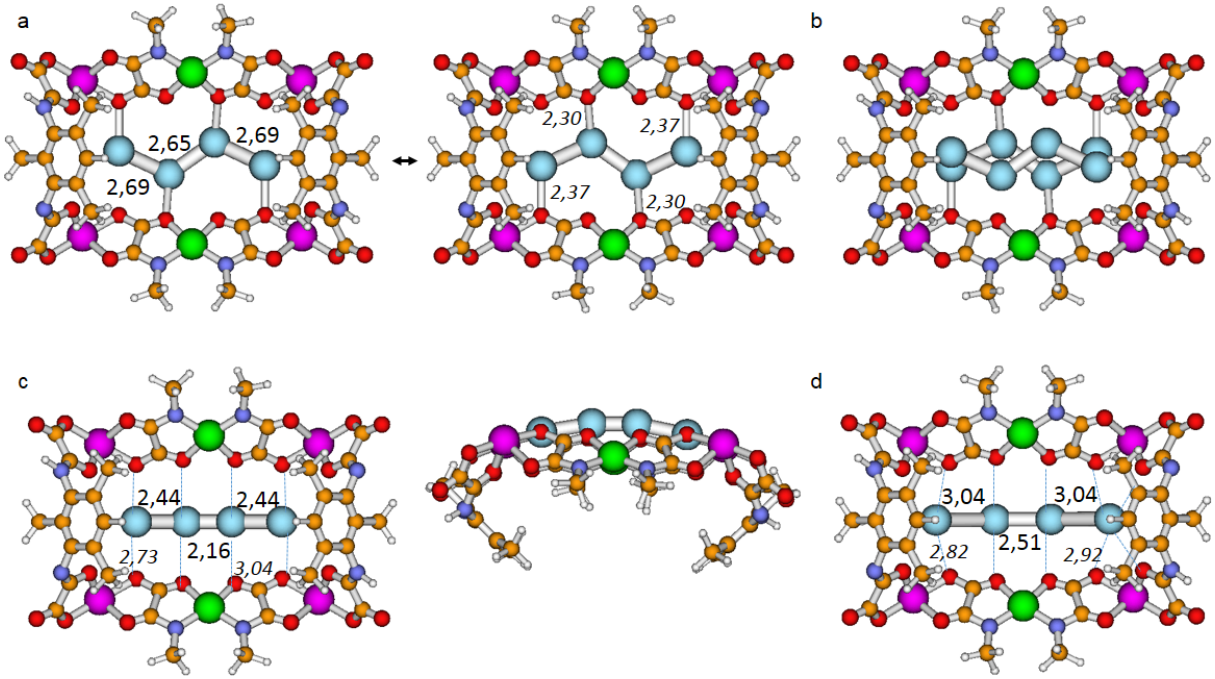

TABLE 1 Catalytic results for Buchner reactions and structures of the Pd complexes tested 10a–f.

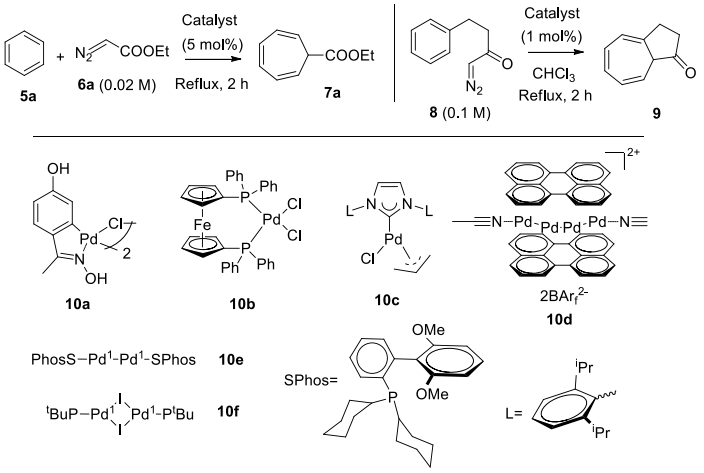

Entry	Catalyst	Yield 7a (%)	Yield 9 (%)
1	$Pd(OAc)_2$	9	<1
2	$PdCl_2$	15	<1
3	$PdCl_2(NH_3)_4 \cdot H_2O$	<5	<1
4	$Pd(OAc)_2$phen	7	<1
5	$PdCl_2(PhCN)_2$	<5	<1
6	$PdCl_2(PPh_3)_2$	11	<1
7	Pd_2dba_3	17	4
8	Nájera´s complex **10a**	<5	<1
9	Ferrocene–Pd^{2+} **10b**	<5	<1
10	Pd–NHC complex **10c**	<5	<1
11	Pd^0 black	9	<1
12	Pd^{2+}–C (5 wt%)	<5	<1
13	Pd^0–C (5 wt%)	<5	<1
14	Pd^0–Al_2O_3	<5	<1
15	Pd^{2+}–MgO	<5	<1
16	Pd^0–MgO	<5	<1
17	Pd^{2+}–HY	<5	1
18	Pd^{2+}–NaY	<5	<1
19	$[Pd(NH_3)_4]^{2+}$–NaY	<5	<1
20	Pd^0–NaY	<5	<1
21	$[Pd(NH_3)_4]^{2+}$–ZSM5	<5	<1
22	Pd^0–HZSM5	<5	<1
23	Pd^{2+}–KL	14	3
24	Pd^0–KL	34	4
25	Pd^{2+}–Mordenite	18	1
26	Pd^0–Mordenite	26	2
27	**3**	**68**	**17**
28	**4**	**75**	**57**
29	Perylene–Pd_4^{2+} **10d**	<5	<1
30	Barder´s complex **10e**	<5	<1
31	(^{t}Bu$_3$PPdI)$_2$ **10f**	<5	<1
32[a]	**4** (0.5 mol%)	**53 (91)**	**39 (71)**
33	$Rh_2(OAc)_4$ (0.5 mol%)	52 (71)	83 (99)

FIGURE 4 Scope and catalytic results.

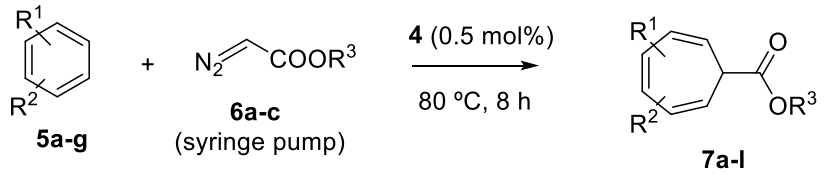

R^1	R^2	R^3	Product	Yield (%)	R^1	R^2	R^3	Product	Yield (%)
H	H	Et	**7a**	91	OMe	H	Et	**7g**	92
Me	H	Et	**7b**	57	OMe	H	^{t}Bu	**7h**	46
Me	Me	Et	**7c**	64	H	H	Bn	**7i**	73
F	H	Et	**7d**	78	Me	H	Bn	**7j**	70
CF_3	H	Et	**7e**	48	OMe	H	Bn	**7k**	95
H	H	^{t}Bu	**7f**	32	F	H	Bn	**7l**	65

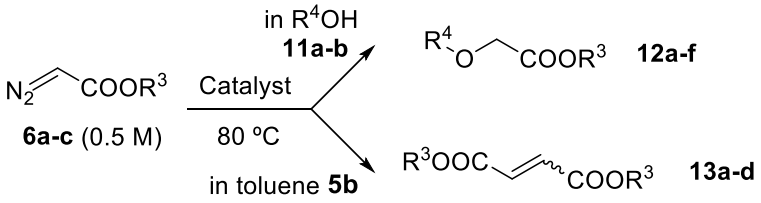

R^3	R^4	Catalyst (mol%)	Time (min)	Product	Yield (%)	*E/Z*
Me	Me	Pd_2dba_3 (0.5)	10	**12a**	72	-
Me	-			**13a**	10	40/60
Me	Me	**10f** (0.5)		**12a**	59	-
Me	-			**13a**	15	47/53
Me	Me	Pd^0-KL (0.5)		**12a**	53	-
Me	-			**13a**	21	52/48
Me	Me	Pd^0-Mor (0.5)		**12a**	44	-
Me	-			**13a**	6	50/50
Me	Me	**4** (0.5)		**12a**	98	-
		4 (0.005)	120		99	- (TON= 49500)
		4 (0.001)			65	- (TON= 65000)
Me	-	**4** (0.5)	10	**13a**	95	50/50
		4 (0.005)	120		96	50/50
		4 (0.001)			93	50/50 (TON= 93000)
Me	^{t}Amyl	**4** (0.005)		**12b**	74	
^{t}Bu	Me			**12c**	88	
Bn	Me			**12d**	96	
Bn	^{t}Amyl			**12e**	85	
8	CD_3OD	**4** (0.5)		**12f**	99	-
^{t}Bu	-	**4** (0.005)		**13b**	78	50/50
Bn	-			**13c**	97	65/35
8	-	**4** (0.05)		**13d**	98	50/50

FIGURE 5 Proposed mechanism for Pd_4 catalysed intermolecular Buchner reaction.